ISSN 1063-7761, Journal of Experimental and Theoretical Physics, 2023, Vol. 137, No. 5, pp. 656–663. © Pleiades Publishing, Ltd., 2023.
Russian Text © The Author(s), 2023, published in Zhurnal Eksperimental'noi i Teoreticheskoi Fiziki, 2023, Vol. 164, No. 5, pp. 761–769.

SOLIDS AND LIQUIDS

Zeeman Splitting of Excitons in GaAs/AlGaAs Quantum Wells in the Faraday Geometry

P. S. Grigoryev[a,*], M. A. Chukeev[a], V. A. Lovtcius[b], Yu. P. Efimov[b], and S. A. Eliseev[b]

[a] *Spin Optics Laboratory, St. Petersburg State University, St. Petersburg, 198504 Russia*

[b] *Resource Center "Nanophotonics," St. Petersburg State University, St. Petersburg, 198504 Russia*

**e-mail: f.grigoriev@spbu.ru*

Received May 18, 2023; revised June 2, 2023; accepted June 5, 2023

Abstract—The Zeeman splitting in the GaAs/AlGaAs heterostructure is investigated experimentally. Numerical analysis performed for the wavefunctions of exciton states, which takes into account the bands of heavy holes, light holes, and the band split by the spin–orbit interaction, is the quantitative agreement with experimental data both for an exciton with a heavy hole and for that with a light hole. It is shown that for explaining the experimental values of the Zeeman splitting in the quantum well under investigation, it is necessary to take into account both the Coulomb interaction and the contribution from the three bands in the valence band. The effect of screening of exciton states by a 2D gas of electrons with concentration $n \approx 10^9$ cm^{-2} is described. Numerical calculations are performed for a large range of quantum well widths and aluminum concentrations in barriers; the chart of the dependence of the effective g factor on these parameters is plotted for magnetic field $B = 5$ T.

DOI: 10.1134/S1063776123110134

1. INTRODUCTION

Analysis of magnetic excitons in GaAs/AlGaAs quantum wells (QWs) [1–4] has revealed the nonlinearity of exciton state splitting in a magnetic field. This nonlinearity can be explained by the clearly manifested effect of renormalization of the g factor (a change in the Zeeman splitting of a free charge carrier primarily under the influence of adjacent bands in the semiconductor). For example, the simple conduction band in GaAs makes it possible to describe the effect of g factor renormalization by the Roth expression [5]. The distances to adjacent bands appearing in this expression vary in GaAs/AlGaAs QWs due to size quantization, which leads to a change in the renormalization effect [6–8] that has been measured experimentally from the Faraday rotation signal. The magnitude of this effect is small to the extent of the ratio of the size quantization energy to the distance to adjacent bands.

Apart from the electron, the behavior of an exciton in a magnetic field is determined by the hole. The approach to the valence band, which is analogous to the Roth formula, makes it possible to obtain parameter κ determining the energy of interaction of the hole angular momentum with the magnetic field with the account for the effect of the nearest bands [9]. However, this parameter does not include the interaction of the bands of heavy holes, light holes, and the spin-split band with one another. Therefore, this parameter determines the "bare" g factor of holes, which is subjected to subsequent renormalization due to the interaction of the three aforementioned bands. Closely spaced bands of heavy and light holes make a larger contribution to the renormalization of the "bare" value of the g factor; however, as will be shown below, the inclusion of the effect of the spin-split band is required for a comprehensive description of the exciton g factor.

Finally, the Zeeman splitting of the exciton state differs from the simple sum of splittings for electron and hole bands. For wide quantum wells, the exciton wavefunction is formed as a standing wave and can be described approximately by the wavevector of the exciton center of mass. In such quantum wells, the dependence of renormalized exciton g factor on the wavevector for quantum wells based on GaAs, CdTe, and ZnSe was demonstrated [10–14]. In these publications, the value of the g factor was described more or less successfully by the mixing of the heavy and the light holes in the valence band. Nevertheless, a simpler model proposed in [10–13], which presumes a factorizable exciton wavefunction with the separation of the center-of-mass motion from the relative motion of the electron and the hole, cannot claim to a description of the variation of the g factor with a magnetic field due to the variation of mixing. More complicated models [14] involve numerical microscopic interaction of the exciton wavefunction, which, in particular, reflects the compression of the exciton wavefunction by the mag-

netic field and, hence, can describe the behavior of the exciton energy in a magnetic field more comprehensively, including the Zeeman splitting under the effect of the *g*-factor renormalization.

The pioneering works devoted to analysis of excitons in typical quantum wells (of width 5–20 nm) [1–4] are based on the calculation of the size quantization levels of charge carriers, for which then the energy correction due to the Coulomb interaction is calculated. Nevertheless, the contribution of exciton effects to the renormalization of the *g* factor in such systems is also significant [15]. The inclusion of exciton effects as a correction often turns out to be insufficiently accurate. This follows from the considerable difference between the experimentally obtained values of the exciton *g* factor and the numerically obtained values. The discrepancy is also preserved in the attempt at taking into account additional mixing appearing due to the crystal symmetry breaking at the QW boundaries [16]. Symmetry considerations lead to the conclusion that such a mixing is possible, but, unfortunately, fail to estimate its value. In [15, 16], the mixing is characterized by parameter $t_{lh} = 0.5$; however, the values of the *g* factor calculated in these works are only in satisfactory agreement with experimental values. At present, the actual value of this parameter is unknown, and additional measurements and refined models are required for a reliable determination of the magnitude of this effect.

On the other hand, the experimental data in the literature are diversified and unreliable. For example, in early publications [1–4], the half-width at the half-amplitude of the resonances under investigation is seldom smaller than 1 meV, which renders the observation of exciton state splitting in fields lower than 2 T rather unreliable. In addition, as shown in [17], even a low concentration of a 2D electron gas (2DEG) (approximately, 5×10^9 cm^{-2}) can screen the Coulomb potential in the exciton. In the case of screening, the exciton wavefunction also changes, which, in turn, changes the Zeeman splitting renormalization effect. This effect is also illustrated in this study.

Finally, the Zeeman splitting of an exciton with a light hole can demonstrate strong nonlinearity in the case of anti-intersection of this state with the excited states of an exciton with a heavy hole [4, 16]. This effect also varies with the QW width and must be manifested in quantum wells with a width smaller than 14 nm for an aluminum concentration in barriers of 30%. Such an anti-intersection additionally complicates experimental investigations and practically rules out the description of splitting of the exciton resonance with the help of a single *g* factor parameter for an exciton with a light hole.

Therefore, a detailed experimental investigation of the behavior of exciton resonances in typical GaAs/AlGaAs QWs with a width from 5 to 30 nm using high-quality heterostructures that are available today. Such an investigation must be accompanied with microscopic numerical calculations of the exciton wavefunctions. This study is a first step in this direction. We have analyzed a high-quality heterostructure with a quantum well of width 14 nm with a low aluminum concentration (about 3%) in barriers. The low aluminum concentration has made it possible to disregard the effects of discontinuities in effective masses [18] and permittivities [19] at the QW boundaries. The relatively low barriers also allow one to disregard additional mixing of bands in the valence band because of symmetry breaking at the QW boundaries [16]. We succeeded in obtaining a reliable description of the *g* factor for an exciton with a heavy hole as well as for that with a light hole. For this, we have taken into account in numerical calculation the mixing of bands for heavy holes, light holes, as well as the spin-orbit-split band.

The article has the following structure: in Section 2, details of the numerical method are described, as well as the details of the experimental method used in this study. Section 3 contains the description of the results and comparison of the numerically obtained exciton energies with experimental values. In Section 4, detailed analysis of the results is performed, while in Section 5, our results are generalized and summarized.

2. METHODS

We have used a specially developed numerical method for obtaining the wavefunctions and energies of exciton states for analyzing the experimentally obtained values of exciton transition energies. We have measured the reflection spectra of the $GaAs/Al_{0.03}Ga_{0.93}As$ heterostructure with a quantum well having a nominal width of 14 nm. These spectra are shown in Fig. 1. The heterostructure is characterized by a high crystal quality. In particular, this is manifested in comparable values of the radiative and nonradiative broadenings of the exciton resonance line in the reflection spectra. As in our previous publications, we analyze the reflection spectra by fitting the measured spectra with the help of expressions

$$R = \left| \frac{r_b + e^{i\phi} r_{QW}}{1 + r_b e^{i\phi} r_{QW}} \right|^2, \quad (1)$$

$$r_{QW} = \sum_j \frac{i\hbar\Gamma_{0j}}{\omega - \omega_j + i\hbar(\Gamma_{0j} + \Gamma_j)}, \quad (2)$$

where r_b is the background amplitude reflectance, r_{QW} is the contribution to the reflection coefficient of exciton resonances, each of which has energy ω_j, radiative broadening $\hbar\Gamma_{0j}$, and nonradiative broadening $\hbar\Gamma_j$. Quantity ϕ is the phase shift between light reflected from the heterostructure surface and light reflected from the quantum well. The stage-by-stage derivation

of these expressions was described in monograph [20]. In this study, we observed in experiments the resonances of excitons with a heavy hole, light hole, as well as the states of trions. The sums of the contributions from these resonances is described by formula (2). The applicability of these expressions also confirms the high quality of the sample under investigation. Indeed, the expressions disregard the nonuniform broadening of resonances, and their ability to describe accurately the observed spectra indicates that such broadening is negligibly small as compared to the uniform broadening of resonances.

The experimental spectra for the samples at temperature $T = 1.2$ K, which have been measured for two circular polarizations, are shown in Fig. 1. Exciton resonances for excitons with a heavy and a light hole are denoted by X_{hh} and X_{lh}, respectively. In a magnetic field, these resonances experience a diamagnetic shift and the Zeeman splitting, which is manifested more clearly for the resonance of an exciton with a light hole. In addition, two more resonances with energies lower than the energy of an exciton with a heavy hole are observed; we ascribe these resonances to trion states with the singlet and triplet configurations.

The experimental data were interpreted using numerical simulation. The numerical method developed earlier [14, 21–24] makes it possible to obtain the solution to the Schrödinger equation for an exciton in a quantum well and takes into account the effect of mixing of bands of heavy and light holes. This technique employs the finite-difference method for obtaining a large sparse matrix corresponding to the exciton Hamiltonian. This matrix is partly diagonalized using the Arnoldi algorithm. The approach to constructing the matrix based on the Luttinger Hamiltonian was described in detail [24]. For a better agreement with experiment, the Hamiltonian in this study has been extended and also includes the band split by the spin-orbit interaction. The structure of such a Hamiltonian for the valence band was described in monograph [25]. The total exciton Hamiltonian was written in form

$$H_{\text{ex}} = H_c + H_v - \frac{e^2}{\varepsilon r} + U(z_e, z_h), \qquad (3)$$

where H_c describes the conduction band, H_v describes the valence band, while the third and fourth terms describe the Coulomb interaction and the QW potential (e is the electron charge, ε is the permittivity of GaAs, r is the distance between the electron and the hole, and $U(z_e, z_h)$ is the rectangular potential of a quantum well with electron and hole coordinates z_e and z_h along the heterostructure growth axis). Analogously to the approach used in [24], the first, third, and fourth terms in expression (3) appear in matrix form H_{ex} on the diagonal. The matrix form H_{ex} itself has dimension 6×6, and its structure follows from the

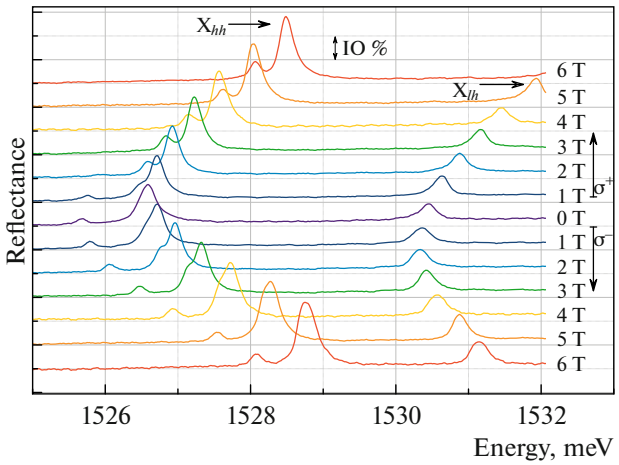

Fig. 1. Reflection spectra of a heterostructure with a GaAs/AlGaAs quantum well of nominal width 14 nm in a magnetic field of up to 6 T in two circular polarizations. X_{hh} and X_{lh} mark the position of the exciton resonance with a heavy and a light hole, respectively.

structure of H_v describing the behavior of a hole in the valence band.

A transition to the coordinates (ρ, ϕ) of the relative motion and (X, Y) of the center of mass in the QW plane corresponds to the cylindrical symmetry of the diagonal part of the Hamiltonian and makes it possible to separate the center-of-mass coordinates in the QW plane and to use an ansatz of form

$$\psi = \exp\left[i\frac{eB}{2c\hbar}(Yx - Xy)\right]\exp(ik_\phi\phi)\psi(z_e, z_h, \rho), \qquad (4)$$

where $x = \rho\cos\phi$ and $y = \rho\sin\phi$. After the substitution of such an ansatz, the Hamiltonian becomes infinitely large and consists of the 6×6 blocks of the initial Hamiltonian represented in the basis of functions $\exp(ik_\phi\phi)$, where ϕ is the angular coordinate of the relative motion of an exciton in the QW plane and k_ϕ are the integer values of the exciton angular momentum projection. We have used a limited set of such functions and composed the Hamiltonian matrix in a limited basis. Following the notation used on [25], we can write matrix H_v in form

$$H_v = \begin{pmatrix} F & H & I & I & \frac{iH}{\sqrt{2}} & -i\sqrt{2}I & -i\sqrt{2}I \\ & G & 0 & 0 & 0 & 0 & 0 \\ & & G & 0 & 0 & 0 & 0 \\ & & & G & 0 & 0 & 0 \\ & & & & S & 0 & 0 \\ & & & & & S & 0 \\ & & & & & & S \end{pmatrix}, \qquad (5)$$

in this case, the limited basis is characterized by a set of numbers k_ϕ: (0, 1, 2, −2, 1, 2, −2), which corre-

spond to angular momentum projections for a hole (3/2, 1/2, −1/2, −1/2, 1/2, −1/2, −1/2). In this notation, the diagonal is treated as complex conjugate operators. Operator $S = (F + G)/2 + \Delta$, where $\Delta = 341$ meV is the spin-orbit splitting, describes the hole states in the spin-orbit-split band. The operators themselves are expressed in terms of the Luttinger parameters as

$$H = \frac{\sqrt{3}\gamma_3\hbar^2}{m_0}(k_y k_z + ik_x k_z), \quad (6)$$

$$I = \frac{1}{\sqrt{12}}\left(\frac{2\gamma_2\hbar^2}{m_0}(k_x^2 - k_y^2) - 2i\frac{\hbar^2\sqrt{3}\gamma_3}{\sqrt{2}m_0}k_x k_y\right), \quad (7)$$

where k_x, k_y, k_z are the components of the generalized momentum operator for the hole and m_0 is the electron mass. For numerical calculations, components k_x, k_y, k_z were represented in coordinate system (X, Y, ρ, ϕ, z_e, z_h). The Luttinger parameters in numerical calculations have the following values: $\gamma_1 = 6.98$, $\gamma_2 = 2.06$, $\gamma_3 = 2.9$, and $\kappa = -1.2$. In the numerical technique used here, the generalized momentum was written with the vector potential in the symmetric gauge with a magnetic field directed along the z axis. The form of operators F and G in terms of the Luttinger parameters was given in [24]. These operators are the diagonal components of the Luttinger Hamiltonian.

Strictly speaking, the coefficients in operators F and G in the composition of operator S differ from the Luttinger parameters to the extent of the difference of the energy gaps between the spin-split band and the upper conduction bands for heavy and light holes. A more rigorous model must stem from the 14-band model described in [16] and must use the parameterization of this model, which corresponds to the experimentally determined values of effective masses in the bands of heavy and light holes.

The logics of constructing the limited basis is dictated by the selection rules in number k_ϕ, and the basis is composed of an optically active state of a heavy-hole exciton and a set of states of a light-hole exciton and the exciton of the spin-orbit-split band with values of $k_\phi = 1, \pm 2$, which are admixed first of all. In this study, we omit the operators mixing the light-hole states of an exciton with an exciton in the spin-orbit-split band and do not consider either the mixing because of the symmetry breaking at the QW boundary described in [16].

In the approach used here, matrix H_v for a light-hole exciton has form

$$H_v = \begin{pmatrix} G & H^* & I & I & \frac{(G-F)i}{\sqrt{2}} & i\sqrt{\frac{3}{2}}H \\ & F & 0 & 0 & 0 & 0 \\ & & F & 0 & 0 & 0 \\ & & & F & 0 & 0 \\ & & & & S & 0 \\ & & & & & S \end{pmatrix} \quad (8)$$

with a set of numbers k_ϕ (0, −1, 2, −2, 0, 1) for the light-hole state and the hole angular momentum projections (1/2, 3/2, −3/2, −3/2, 1/2, 1/2). For all states, the electron spin projections in the conduction band are assumed to be $\sigma_z = -1/2$ for expression (5) and $\sigma_z = 1/2$ for expression (8). Therefore, the operator in the left upper corner describes optically active states of a heavy exciton in expression (5) and a light exciton in expression (8). For the light-hole exciton, we also ignore the operators mixing the states of the heavy-hole exciton with the states of the exciton in the spin-orbit-split band.

The results of numerical simulation will be compared below with experimental data in Fig. 1.

3. RESULTS

Before considering the results of our analysis, it is worth to pay attention to the following feature of the measured reflection spectra. Figure 2 shows the reflection spectra in field $B = 3$ T, which have been measured for opposite circular polarizations. The measurements were taken in two regimes (with 2DEG generation and without it). The 2DEG pumping was performed by light from an incandescent lamp exciting the reflection spectrum with energy exceeding 1549 meV. The measurements without 2DEG pumping were performed using an interference filter cutting off radiation with energy exceeding 1549 meV. Comparison of two spectra shows that 2DEG leads to an energy shift of exciton states; this shift for the exciton state with a light hole (0.11 meV) exceeds the shift for a heavy-hole exciton (0.04 meV). The presence of 2DEG in the quantum well leads to the formation of trion states [26]: the singlet state is observed in the σ^- polarization, while the triplet state is manifested in two polarizations; however, the state in the σ^+ polarization becomes more distant from the exciton state upon an increase in the magnetic field, while these states in the σ^- polarization merge into one as shown in Fig. 1.

The screening of exciton states in GaAs/AlGaAs quantum wells was considered in [17], where the dependences of the exciton binding energy and its oscillator strength on dimensionless parameter $r_s = 1/a_B\sqrt{2\pi N_s}$ were obtained, where a_B is the exciton Bohr radius and N_s is the 2DEG concentration. To analyze this phenomenon, we fitted the reflection spectra using the technique described in [24] and compared the energies of exciton states with the results of numerical calculations shown in Fig. 3. As regards the position of exciton resonances, the measured reflection spectra correlate with the results of calculation for a quantum well of width 12 nm. Such a difference from the nominal width is explained by the inhomogeneity of the experimental sample and amounts for this sample to 7 monolayers relative to the point of measurement of the heterostructure growth rate by the

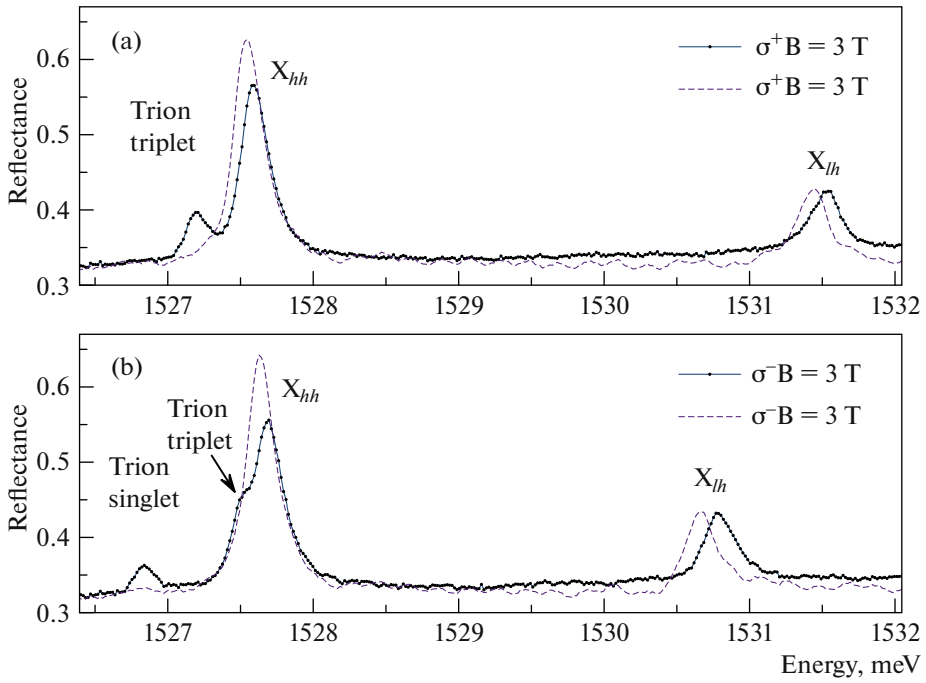

Fig. 2. Reflection spectra of a heterostructure with a GaAs/AlGaAs quantum well of nominal width 14 nm: (a) σ^+ polarization; (b) σ^- polarization. Dashed curves, in contrast to solid curves, are the data measured without injecting the 2D electron gas. In the presence of 2DEG, trion states denoted as trion singlet and trion triplet are manifested.

method of diffraction of fast electrons. As shown in Fig. 3, the results of numerical calculation differ from the experimentally obtained energies of exciton resonances in the range of low fields. Measurements in field $B = 3$ T make it possible to connect the result of the numerical calculation with the energies of exciton states in the screening conditions and to estimate the value of screening. In zero magnetic field, the screening was $\Delta E_{scr} = 0.09$ meV for an exciton with a heavy hole and $\Delta E_{scr} = 0.27$ meV for an exciton with a light hole. Using the results obtained in [17], we have estimated the 2DEG concentration corresponding to such screening and found that $N_s \approx 10^9$ cm^{-2}. The screening decreases with the magnetic field; however, quantitative analysis of this effect requires additional experimental and theoretical investigations.

It should be noted that a method for determining the 2DEG concentration in a quantum well in heterostructures based on types II–VI semiconductors from the relation between radiative broadenings of the trion and the exciton was proposed and implemented in [27]. In [28], the concentration in a system with a WSe_2 monolayer was successfully connected with the energy difference between the states of the trion and the exciton. These systems ensure a high binding energy for the exciton and the trion, which simplifies the measurement of trion states in experiment. For implementing analogous approaches for GaAs-based heterostructures, high-quality samples and low temperatures are required. For example, in the heterostructure investigated in this study, the trion signal in the reflection vanishes almost completely even at $T = 4$ K.

As can be seen from Fig. 4, the Zeeman splitting of trion states differs from the splitting of a heavy-hole exciton in the triplet state, but does not differ significantly for the singlet state. Probably, the difference of the trion wavefunction from the exciton wavefunction leads to a change in the trion g factor because of the effect of its renormalization.

Theoretical analysis of a 2D trion shows that a negatively charged trion should not be bound in the triplet configuration in the GaAs QW [29]. However, this conclusion has not been confirmed experimentally. For example, the experimental observation of a negative triplet trion in field $B = 2$ T was described in [30]. In our measurements, the triplet state was observed even in field $B = 1$ T.

In Fig. 4, the results of numerical calculation are compared with experimentally obtained energies of exciton and trion resonances. For convenience, the results of numerical calculations for the exciton are shifted by 100 μeV. The positions of the levels of trion states in Fig. 4 are shown by dashed curves that repeat the curve for the exciton, but are shifted by 0.15 meV (triplet state) and by 0.7 meV (singlet state).

In Fig. 4, two models are compared: the Luttinger Hamiltonian used in [24] and the extended model

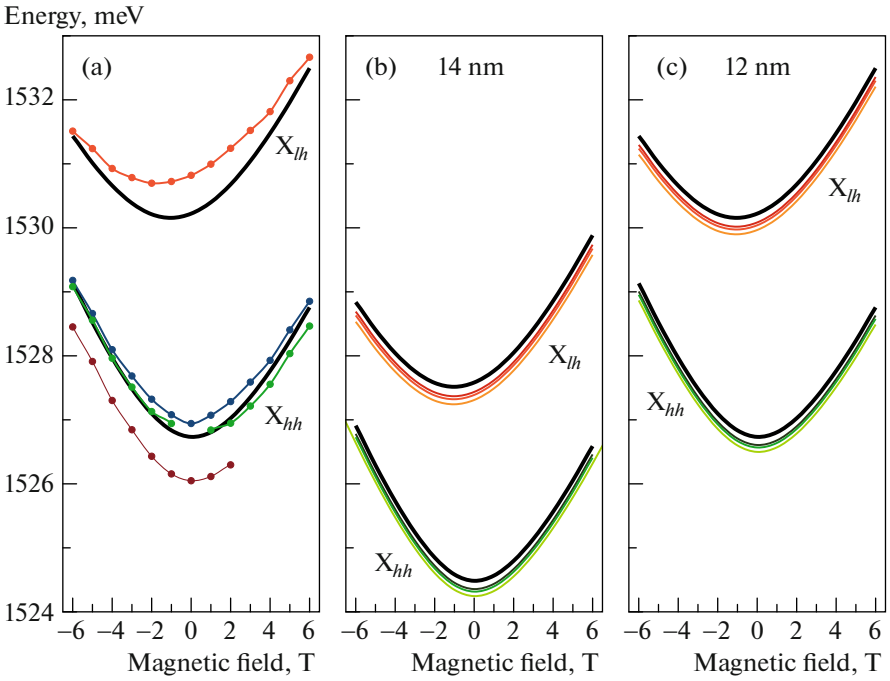

Fig. 3. (a) Experimentally obtained energies of states of an exciton with a heavy hole (blue dots), an exciton with a light hole (red dots), as well as the triplet (green dots) and singlet (purple dots) states of a trion in a GaAs/AlGaAs quantum well of width 14 nm. (b, c) Results of numerical calculation of exciton states for quantum wells of width (b) 14 nm and (c) 12 nm. Colored curves in (b) and (c) show the results of calculation corresponding characteristic grid pitches of 1.27 nm, 1.08 nm, and 0.93 nm. Black curves are the results of extrapolation of numerical results from the grid pitch. Black curves in (a) duplicate black curves in (c) for convenience of comparison of the results of calculation with experimental data.

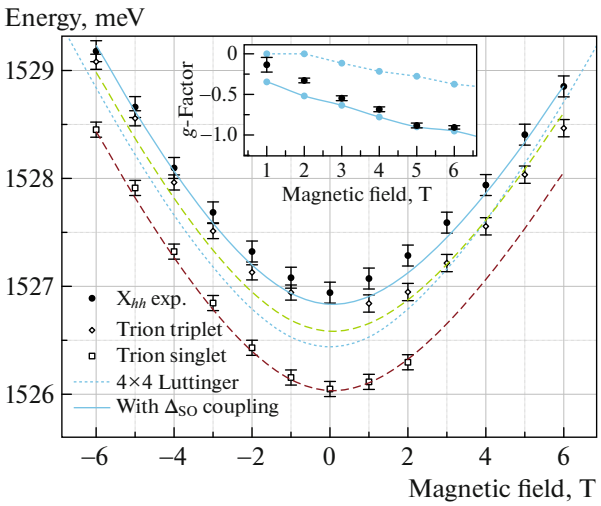

Fig. 4. Energies of states of an exciton with a heavy hole, as well as the triplet and singlet states of a trion in a GaAs/AlGaAs quantum well of nominal width 14 nm. Short-dash curve is the result of numerical calculation with account for only the mixing of heavy-hole and light-hole excitons; solid curve is the result of calculation with account for the spin-orbit-split band in the valence band; long-dash curve illustrates the behavior of trion states, which is expected from calculation. The inset shows the Zeeman splitting of the exciton state as a function of the magnetic field, which is expressed in terms of the g factor in accordance with formula $\Delta E = g\mu_B$.

with account for the spin–orbit splitting of the band. The inset to the figure shows the value of the effective g factor as the proportionality factor between the magnetic field and the Zeeman splitting of the state of a heavy-hole exciton. Comparison of the results of numerical calculations with the experimentally obtained values (bullets) shows a better agreement for a more comprehensive model in which the effect of the band split by the spin–orbit interaction is taken into account.

The errors demonstrated in Fig. 4 indicate the general broadening of the experimentally observed state, but the inset shows a confidence level of 99% obtained from the standard deviation of fitting of experimental spectra, which has been described in detail in [24]. The position of exciton resonances can be determined with standard deviation $\sigma = 1$–4 μeV. Comparison of the most comprehensive calculation with experimental values of the g factor indicates a discrepancy for a low value of the field and good agreement for higher fields. We attribute this discrepancy to the screening effect that affects the wavefunction geometry and, hence, changes the magnitude of the effect of g factor renormalization.

In addition to the effective g factor of an exciton with a heavy hole, we give the value of this parameter for an exciton with a light hole in the upper panel of

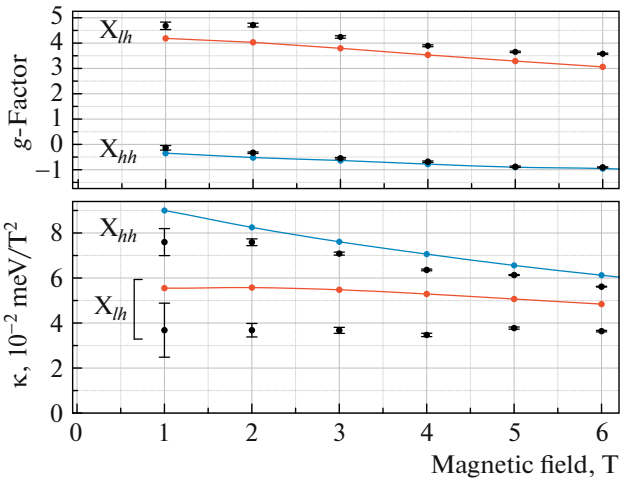

Fig. 5. Comparison of numerically obtained values of the effective g factor and diamagnetic shift constant κ with experimentally obtained values as functions of the magnetic field.

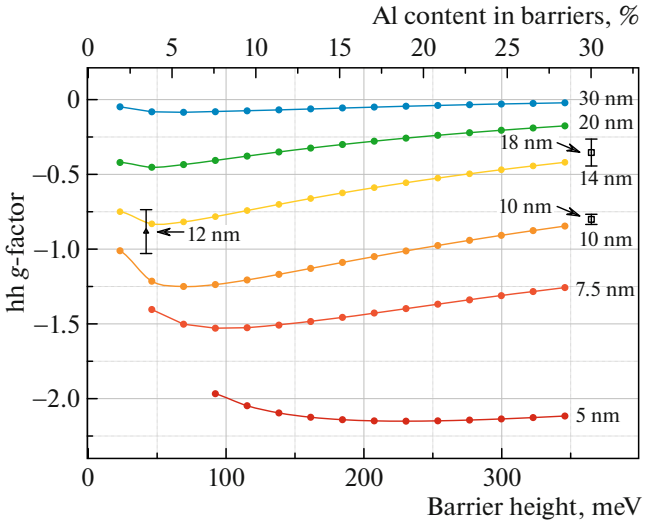

Fig. 6. Numerically obtained value of the g factor of an exciton with a heavy hole for different widths of quantum wells and the aluminum concentrations in the barriers in field $B = 5$ T. Black symbols show experimentally obtained values: (triangle) this work; (light square) [1]; and (filled square) [2].

Fig. 5. The agreement with experiment is generally worse; however, the numerical calculation exactly reconstructs the dependence of the effective g factor on the magnetic field. We define the effective g factor as

$$g(B) = \frac{\Delta E(B)}{\mu_B B}, \tag{9}$$

where ΔE is the Zeeman splitting of the exciton state,.

The lower panel in Fig. 5 shows the effective diamagnetic shift constant κ as a function of magnetic field B, which is defined as

$$\kappa = \frac{E_{\sigma^+}(B) + E_{\sigma^-}(B) - 2E(0)}{2B^2}, \tag{10}$$

where $E_{\sigma^+(\sigma^-)}$ is the energy of the exciton state with polarization $\sigma^+(\sigma^-)$ and $E(0)$ is the exciton energy in zero magnetic field.

We believe that the discrepancy between the numerically obtained values of the diamagnetic shift constant is the result of the change in the exciton screening upon an increase in the magnetic field. The results of calculations are in good agreement with the diamagnetic shifts reported in [1], where apart from data correlating well with experimental values of parameter κ, the data from earlier works deviating towards smaller values are also presented. This may indicate the manifestation of the exciton screening in these works.

4. DISCUSSION

Figure 5 demonstrates a deviation of the diamagnetic shift from the parabolic dependence upon an increase in the magnetic field. Apart from the effect of possible parasitic screening by free charge carriers, this complicates analysis of experimental data and comparison of the results of different investigations.

Finally, in Fig. 6, we represent the results of numerical calculation of the effective g factor of an exciton with a heavy hole for GaAs/AlGaAs QWs in a wide range of aluminum concentrations in barriers and for different QW widths. The data have been obtained for magnetic field $B = 5$ T.

Figure 6 also shows the values obtained in our experiments and available in the literature. The small amount of experimental data can clearly be seen in the figure. Indeed, the values of the g factor as a function of the QW width can belong to a wide range comparable with the range of variation of the effective g factor with the magnetic field. Consistent investigations require a large number of measurements, which must be supported by numerical simulation like that used in this study. However, it is also necessary to take into account the change in the electron g factor [6–8], the jump in effective masses and permittivities at the QW boundaries [18, 19], as well as additional mixing effects associated with symmetry breaking at the QW boundary [16].

5. CONCLUSIONS

The numerical calculation of the exciton stated has revealed good agreement with experimentally observed dependences of the energies of heavy-hole and light-hole excitons. To obtain this result, the numerical calculation of exciton states developed by us earlier [14, 21, 24] has been extended to take into account the effect of the spin-orbit-split band in the

valence band. Comparison of the results of calculations based on the new model with experimentally obtained results demonstrates the existence of the effect of screening of the exciton state in the heterostructure under investigation. This effect was studied theoretically in [17]. Comparison of our results with the results of numerical simulation performed in this study has made it possible to determine the 2DEG concentration, $N_s \approx 10^9$ cm^{-2}. The observed screening for an exciton with a light hole considerably exceeds the screening for an exciton with a heavy hole. The effect of screening decreases with the magnetic field, which substantially reduces the observed value of the diamagnetic shift. This effect is manifested especially clearly for an exciton with a light hole. The numerically obtained values of the effective g factor represented in Fig. 6 for field $B = 5$ T in wide ranges of QW widths and aluminum concentrations are confirmed by experimental data reported in our earlier publications.

ACKNOWLEDGMENTS

The authors are grateful to the Resource Center "Nanophotonics" of the St. Petersburg State University for providing samples and to A. Levantovskii for the MagicPlot software used in data analysis.

FUNDING

This study was supported by the Russian Science Foundation (project no. 21-72-00037, https://rscf.ru/project/21-72-00037/) and the St. Petersburg State University (grant no. 94030557).

CONFLICT OF INTEREST

The authors of this work declare that they have no conflicts of interest.

REFERENCES

1. G. E. W. Bauer and T. Ando, Phys. Rev. B **37**, 3130(R) (1988).
2. H. Wang, M. Jiang, R. Merlin, and D. G. Steel, Phys. Rev. Lett. **69**, 804 (1992).
3. N. J. Traynor, R. J. Warburton, M. J. Snelling, and R. T. Harley, Phys. Rev. B **55**, 15701 (1997).
4. V. B. Timofeev, M. Baier, A. Forkhel, and M. Potemski, JETP Lett. **64**, 57 (1996).
5. L. M. Roth, B. Lax, and S. Zwerdling, Phys. Rev. **114**, 90 (1959).
6. W. Zawadzki, P. Pfeffer, R. Bratschitsch, et al., Phys. Rev. B **78**, 245203 (2008).
7. I. A. Yugova, A. Greilich, D. R. Yakovlev, et al., Phys. Rev. B **75**, 245302 (2007).
8. W. Shichi, T. Ito, M. Ichida, et al., Jpn. J. Appl. Phys. **48**, 063002 (2009).
9. A. A. Kiselev and L. V. Moiseev, Phys. Solid State **38**, 866 (1996).
10. J. J. Davies, D. Wolverson, V. P. Kochereshko, et al., Phys. Rev. Lett. **97**, 187403 (2006).
11. L. C. Smith, J. J. Davies, D. Wolverson, et al., Phys. Rev. B **78**, 085204 (2008).
12. J. J. Davies, L. C. Smith, D. Wolverson, et al., Phys. Rev. B **81**, 085208 (2010).
13. L. C. Smith, J. J. Davies, D. Wolverson, et al., Phys. Rev. B **83**, 155206 (2011).
14. P. S. Grigoryev, O. A. Yugov, S. A. Eliseev, et al., Phys. Rev. B **93**, 205425 (2016).
15. M. V. Durnev, Phys. Solid State **56**, 1416 (2014).
16. M. V. Durnev, M. M. Glazov, and E. L. Ivchenko, Phys. E (Amsterdam, Neth.) **44**, 797 (2012).
17. D. V. Kulakovskii, S. I. Gubarev, and Yu. E. Lozovik, JETP Lett. **74**, 118 (2001).
18. R. C. Iotti and L. C. Andreani, Phys. Rev. B **56**, 3922 (1997).
19. A. D'Andrea, N. Tomassini, L. Ferrari, et al., J. Appl. Phys. **83**, 7920 (1998).
20. E. L. Ivchenko, *Optical Spectroscopy of Semiconductor Nanostructures* (Springer, New York, 2004).
21. E. S. Khramtsov, P. A. Belov, P. S. Grigoryev, et al., J. Appl. Phys. **119**, 184301 (2016).
22. P. S. Grigoryev, V. G. Davydov, S. A. Eliseev, et al., Phys. Rev. B **96**, 155404 (2017).
23. P. A. Belov, Phys. E **112**, 96 (2019).
24. M. A. Chukeev, A. S. Kurdyubov, V. A. Lovtcius, et al., arXiv: 2304.04988 (2023).
25. G. L. Bir and G. E. Pikus, *Symmetry and Stain-Induced Effects in Semiconductors* (Nauka, Moscow, 1972; Wiley, New York, 1975).
26. R. T. Phillips, G. C. Nixon, T. Fujita, et al., Solid State Commun. **98**, 287 (1996).
27. G. V. Astakhov, V. P. Kochereshko, D. R. Yakovlev, et al., Phys. Rev. B **65**, 115310 (2002).
28. K. Wagner, E. Wietek, J. D. Ziegler, et al., Phys. Rev. Lett. **125**, 267401 (2020).
29. R. A. Sergeev and R. A. Suris, Phys. Status Solidi B **227**, 387 (2001).
30. I. Bar-Joseph, Semicond Sci. Technol. **20**, R29 (2005).

Translated by N. Wadhwa

Publisher's Note. Pleiades Publishing remains neutral with regard to jurisdictional claims in published maps and institutional affiliations.